


RESEARCH ARTICLE

Tin-doped bismuth dendrites for highly efficient electrocatalytic reduction of CO₂ by using bipolar membrane in ultrathin liquid reactor

Luwei Peng^{1,2,3} | Changsheng Chen³ | Ruinan He^{1,2} | Nengneng Xu^{1,2} | Jinli Qiao^{1,2} | Zezhou Lin³ | Ye Zhu³ | Haitao Huang³ 

¹State Key Laboratory for Modification of Chemical Fibers and Polymer Materials, College of Materials Science and Engineering, Donghua University, Shanghai, China

²Shanghai Institute of Pollution Control and Ecological Security, Shanghai, China

³Department of Applied Physics and Research Institute for Smart Energy, Hong Kong Polytechnic University, Kowloon, Hong Kong, China

Correspondence

Haitao Huang, Department of Applied Physics and Research Institute for Smart Energy, Hong Kong Polytechnic University, Kowloon, Hong Kong, China. Email: aphhuang@polyu.edu.hk

Jinli Qiao, State Key Laboratory for Modification of Chemical Fibers and Polymer Materials, College of Materials Science and Engineering, Donghua University, Shanghai, China. Shanghai Institute of Pollution Control and Ecological Security, Shanghai, China. Email: qiaojl@dhu.edu.cn

Funding information

Donghua University, Grant/Award Number: CUSF-DH-D-2021036; Hong Kong Polytechnic University, Grant/Award Numbers: YWB6, YWA1; Research Grants Council of the Hong Kong Special Administrative Region, Grant/Award Number: PDFS2122-5S02; Shanghai Science and Technology Committee, Grant/Award Number: 19JC1410500

Abstract

Electrochemical CO₂ reduction reaction is a promising protocol to achieve a carbon-neutral cycle. Herein, we report a general strategy to regulate the growth of Sn-doped Bi dendritic electrode with numerous labyrinthine and porous channels to provide abundant tips, edges, terraces, and low coordination sites for efficient conversion of CO₂ into formate. As a result, the dendritic Sn-doped Bi achieves a high partial current density (30 mA/cm²), a high Faradic efficiency of formate (95.5%), and a long-term durability (>60 h). Most remarkably, the self-made bipolar membrane can effectually prohibit the cross-over of formate from cathode to anode and the oxidization of small organic molecules in anode can promote the production of formate on both anode and cathode sides. This work provides helpful insights to the design of electrocatalysts, bipolar membrane, and ultrathin liquid reactor.

KEYWORDS

bipolar membrane, dendritic morphology, electrochemical CO₂ reduction reaction, Sn-doped Bi electrode, ultrathin liquid reactor

[Correction added on 5 August 2022, after first online publication: "Department of Environmental Sciences" has been removed on the second affiliation. Jinli Qiao has been added on the Correspondence section]

This is an open access article under the terms of the [Creative Commons Attribution](https://creativecommons.org/licenses/by/4.0/) License, which permits use, distribution and reproduction in any medium, provided the original work is properly cited.

© 2022 The Authors. *EcoMat* published by The Hong Kong Polytechnic University and John Wiley & Sons Australia, Ltd.

1 | INTRODUCTION

Electrochemical CO₂ reduction reaction (CO₂RR) to form renewable fuels and industrial chemical stocks by using clean energy (e.g., solar, wind, tidal, and geothermal energies) is a promising protocol to achieve a carbon-neutral energy cycle.¹ Many efforts have been devoted to developing a variety of catalysts for the synthesis of gas and liquid products such as carbon monoxide, methane, ethylene, formic acid, methanol, ethanol, and acetone, etc. Among these products, formic acid as a pharmaceutical and chemical feedstock is deemed to have a huge competitive advantage due to its convenient storage and easy transportation for industry,^{2–4} and as ideal hydrogen carrier and liquid fuel it can also be directly applied in formic acid fuel cells.⁵ Interestingly, various basic metals like In,⁶ Pb,⁷ Sn,⁸ and Bi⁹ are believed to possess high activity and selectivity for converting CO₂ into formate, whereas the precursor of In is very expensive and cannot be metabolized in human organisms, and Pb is environmentally hazardous and toxic.⁹ As a result, Sn and Bi-based catalysts with low cost, low toxicity, and capability of suppressing hydrogen evolution reaction (HER) have been regarded as the best candidates for the adsorption of OCHO* intermediate (an intermediate for formate generation) over the COOH* intermediate (an intermediate for CO generation), thus favoring the production of formate rather than CO.¹⁰

To date, a series of studies about Sn and Bi-based catalysts for CO₂RR focus on the design of specific morphology and microstructure,¹¹ reconstruction of local electronic structure,¹² regulation of multi low coordination sites,¹³ and introduction of surface defects and vacancies.¹⁴ The way to achieve the above objectives is through introducing orbital interactions,¹⁵ oxygen vacancies,¹⁶ sulfur defects,¹⁷ high-index planes,¹⁸ phase boundaries,¹¹ and grain boundaries.² However, to the best of our knowledge, rare efforts have been devoted into developing bimetallic Sn-Bi catalysts with sharp-tip enhancement effect to efficiently convert CO₂ into formate. Actually, for electrocatalytic conversion of CO₂ into CO, it has been proved that gold nanoneedles with tip-enhanced field phenomenon can generate a high local electric field, which in turn concentrates electrolyte cations and further lowers the thermodynamic energy barrier for the electrochemical reduction of CO₂ to CO.¹⁹ Similarly, copper nanoneedles with high surface charge density at tips can concentrate K⁺ near the tips, thus enhancing the efficiency of CO₂RR by adsorbing more CO₂ molecule around the tips.²⁰ These findings suggest that a sharp conical feature plays a significant role in CO₂ catalytic reaction, rendering it a promising strategy for designing efficient catalysts with high local electric fields.

Except for designing novel electrocatalysts, the membrane is also an important factor to consider in a CO₂RR system. There are three types of ionic exchange membranes (cation-exchange, anion-exchange, and bipolar membranes) that have been utilized in CO₂RR. Each type of membrane determines a different ion transport pathway between the cathode and anode. Cation-exchange membrane (such as Nafion 115, 117, and 212) with negatively-charged functional groups allows the movement of positive ions (H⁺) from the anode to the cathode, which would reduce the Faradic efficiency of CO₂RR by favoring the formation of H₂. However, the anion-exchange membrane with positively-charged functional groups facilitates the flow of anions (OH[−], CO₃^{2−}, HCO₃[−]) from the cathode to the anode.²¹ The anion transport pathway is more suitable than the cation one in that the lowered H⁺ concentration around the surface of cathode catalyst suppresses the HER. The main problems of anion-exchange membrane are the high anionic conductivity leading to the product crossover, poor stability and low CO₂ utilization that limit its practical application. Bipolar membrane consisted of an anion-exchange layer and a cation one has been extensively used in water splitting,²² self-humidified fuel cell and electrodialysis because no ions are permitted to penetrate through the membrane,²³ while it is also an emerging breakthrough in the application of CO₂ conversion devices. The benefits of using bipolar membrane under reverse bias are the inhibition of product crossover and the dissociation of water at the interface of anion- and cation-exchange layers, which drives the flow of H⁺ towards cathode and OH[−] towards anode, and keeps a constant pH of both sides.²⁴ The constant pH in anode offers the possibility to apply inexpensive anode catalyst (Ni, Fe, Co-based materials) for stable oxygen evolution reaction (OER). Indeed, the above merits of bipolar membrane give its priority to be assembled into CO₂ electrolyzer flow cell under high current density working condition.²¹

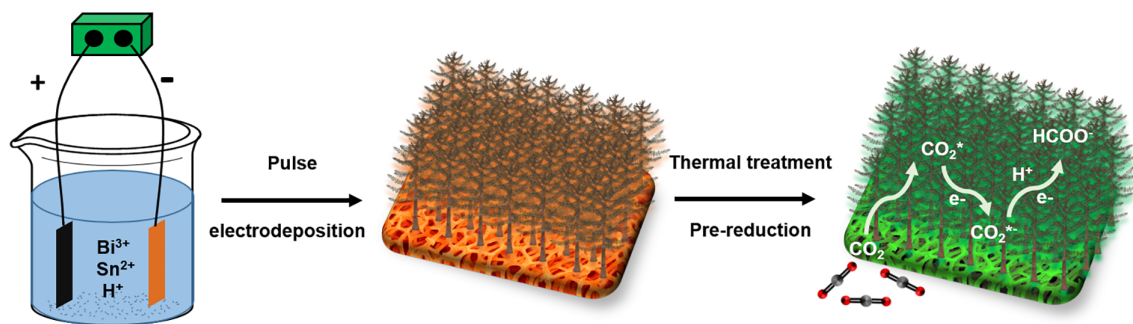
For a typical CO₂RR, there are four key steps: charge transport (electron transport from conductive substrate to electrocatalyst), surface conversion (CO₂ is adsorbed on the surface of catalyst), charge transfer (electron transfer from catalyst surface to CO₂ intermediate), and mass transfer (CO₂ diffuses from electrolyte to catalyst surface and products diffuse in the reverse pathways), while the former two steps depend on the development of highly conductive catalysts with abundant active sites, and the latter two rely on the properties of electrolyte and the optimization of electrolytic cell configuration. As a consequence, except for designing novel Bi and Sn-based catalysts and membranes, designing electrochemical cell with optimum configuration is also indispensable, particularly for industrial

application to achieve the economically viable and technologically competent targets such as cell voltage (<1.8 V), Faradaic efficiency ($>90\%$), current density (>200 mA cm $^{-2}$) and durability (>1000 h).^{25–27} To keep these goals in mind, the currently reported electrolyzer for CO₂RR can be classified into H-type cell,²⁸ polymer membrane flow cell,²⁹ microfluidic flow cell,³⁰ filter-press electrochemical cell,³¹ high pressure cell,³² solid oxide cell and solid electrolyte cell.^{33–35} It is worth noting that a number of factors still need to be considered for a lab-scale CO₂RR cell configuration to be applicable in the forthcoming commercialization and industrial applications. These contain low energy input for both anode reaction and CO₂RR as a full cell, efficient separation of gas and liquid products in cathode compartment, and ideal enlargement of efficient working area.^{25,36}

Herein, we report the growth of a dendritic Sn-doped Bi with stable microstructure and the growth mechanism of this peculiar morphology. The dendritic Sn-doped Bi with multiple high-curvature tips would concentrate K⁺ in aqueous electrolyte and in turn enable the CO₂RR in an ultra-high local electric field. Such dendritic morphology with a great deal of labyrinthine and porous channels can provide abundant tips, edges, terraces, and low coordination sites to function as active sites for highly efficient conversion of CO₂ into liquid products. Combining the above benefits, the dendritic Sn-doped Bi electrode can achieve a considerably high partial current density (30 mA cm $^{-2}$), a high Faradic efficiency of formate (95.55%) and a long-term durability (>60 h). Besides, we also study the effects of membrane and anode reaction, and show that the bipolar membrane can efficiently prohibit the cross-over of formate from cathode to anode. In summary, this work shows the importance of the rational design of novel electrocatalysts as well as efficient bipolar membrane in the development of CO₂RR system for industrial applications in the future.

2 | RESULTS AND DISCUSSION

The Sn-doped Bi (see Experimental Procedures) electrode is prepared via a pulse electrodeposition process followed by thermal treatment and pre-reduction step (Scheme 1). Key to the synthesis is the application of pulse electrodeposition and the introduction of H⁺ in electroplating solution. Scanning electron microscopy (SEM) images in Figure S1A–B show that the Sn-doped Bi consists of typical dendritic microstructures with multiple branches growing on the trunk. The bright field transmission electron microscopy (TEM) image of Sn-doped Bi in Figure 1A shows a dendritic structure with single crystalline orientation (as manifested by the electron diffraction pattern in inset). The as-prepared Sn-doped Bi electrode is then heated at 85°C for 3 h to remove superficial residual from electroplating liquid and stabilize the dendritic morphology. The thermal treatment temperature of 85°C is chosen since it is well below the melting point of Sn and Bi alloy, so that this procedure would not jeopardize the dendritic microstructure. Therefore, no obvious morphological change of Sn-doped Bi is observed after the thermal treatment, except partial oxidation as shown in the mapping images of Figure 1B and Figure S1C,D. An amorphous layer (~ 0.8 nm) can be observed on the tip of dendrite branches from the high-resolution TEM (HRTEM) image (Figure 1C) and bismuth in the inner part of the dendrite can be identified with a lattice spacing of 0.326 nm corresponding to the (10 $\bar{2}$) planes of bismuth. However, when the thermal treatment temperature is increased to 275°C (Figure S2), the dendritic structure of Sn-doped Bi is obviously damaged because of melting. Before CO₂RR detection, the Sn-doped Bi after thermal treatment at 85°C is electrochemically pretreated in 1 M KOH, with an aim to reduce oxidation species and adsorb K⁺. As illustrated in Figures 1D and S3, even if the Sn-doped Bi is sequentially treated by heat and electrochemical treatment, the



SCHEME 1 Schematic illustration of the synthesis process of dendritic Sn-doped Bi electrode and the reaction pathway for formate generation.

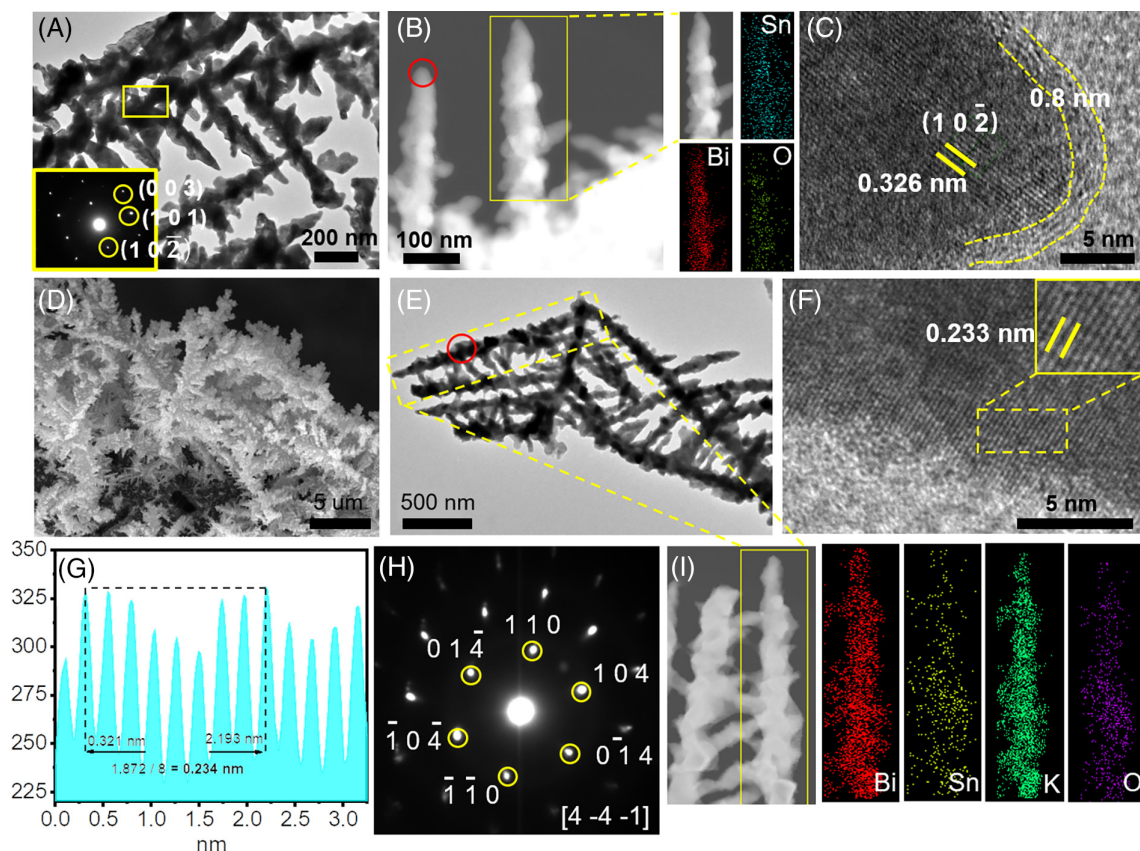


FIGURE 1 (A) TEM image of Sn-doped Bi (before thermal treatment) with zone axis [010]. Inset is the SAED pattern of the region enclosed by the yellow rectangle. (B) TEM and (C) HRTEM images of Sn-doped Bi electrode after thermal treatment at 85°C. The elemental mapping in (B) is taken from the yellow rectangle region and the HRTEM image in (C) is taken from the red circle region in (B). (D) SEM, (E) TEM, and (F) HRTEM images of Sn-doped Bi after electrochemical pre-reduction. Inset in (F) is the enlarged high-resolution image of the yellow dashed rectangle. (G) Line scan intensity profile taken along the atomic layers in the yellow solid rectangle in (F). (H) SAED pattern of Sn-doped Bi with zone axis $[4\bar{4}1]$. (I) TEM elemental mapping results taken from (E)

dendritic morphology of Sn-doped Bi still keeps the same as that without any treatment in Figure S1A. Figure 1E reveals that the branch length of Sn-doped Bi is around 1 μm and the tip radius is below 30 nm. This type of dendritic structure would certainly increase the adsorption of CO_2 intermediate and favor the desorption of CO_2RR products. Moreover, such sharply curved tips with high local electric field would concentrate cations in aqueous electrolyte and in turn facilitate the CO_2RR . Interestingly, the amorphous layer in Figure 1C is hard to observe in the electrochemically treated sample as shown in Figure 1F, demonstrating that the superficial oxidized species of Sn-doped Bi has been reduced. The HRTEM (inset of Figure 1F) reveals a lattice spacing of 0.233 nm, which matches well with that of the (104) planes of bismuth (Figure 1G). The selected area electron diffraction (SAED) pattern in Figure 1H shows a typical single-crystalline structure with hexagonal crystal symmetry along $[4\bar{4}1]$ zone axis, and clear diffractions from the Bi (104) and (110) planes. As shown in Figure 1I,

elemental mapping results display that K is uniformly distributed on the surface of Sn-doped Bi after the electrochemical treatment. The adsorption of K^+ can also be confirmed by the TEM-EDS result in Figure S4.

The pulse electrodeposition mode, comprised of multiple 1 min “on” and 0.5 min “off” cycles in Figure S5, can be used as an effective technique to replenish metal ions close to the growth substrate in “off” cycles. As shown in Figure 2A, the metal ions and protons would firstly move to the cathode under electric field. When the metal cations and protons arrive at the surface of the cathode, electrons would transfer from the cathode to metal ions and protons following the activity sequence of metal in aqueous solution. As the reduction potential of Bi^{3+} and Sn^{2+} is 0.308 and -0.138 V versus SHE (standard hydrogen electrode), respectively, the sequence of getting electrons in aqueous solution is Bi^{3+} , H^+ and Sn^{2+} . Therefore, a depletion region of bismuth cations will be formed near the surface of substrate (Figure 2A) and those Bi^{3+} ions are reduced to

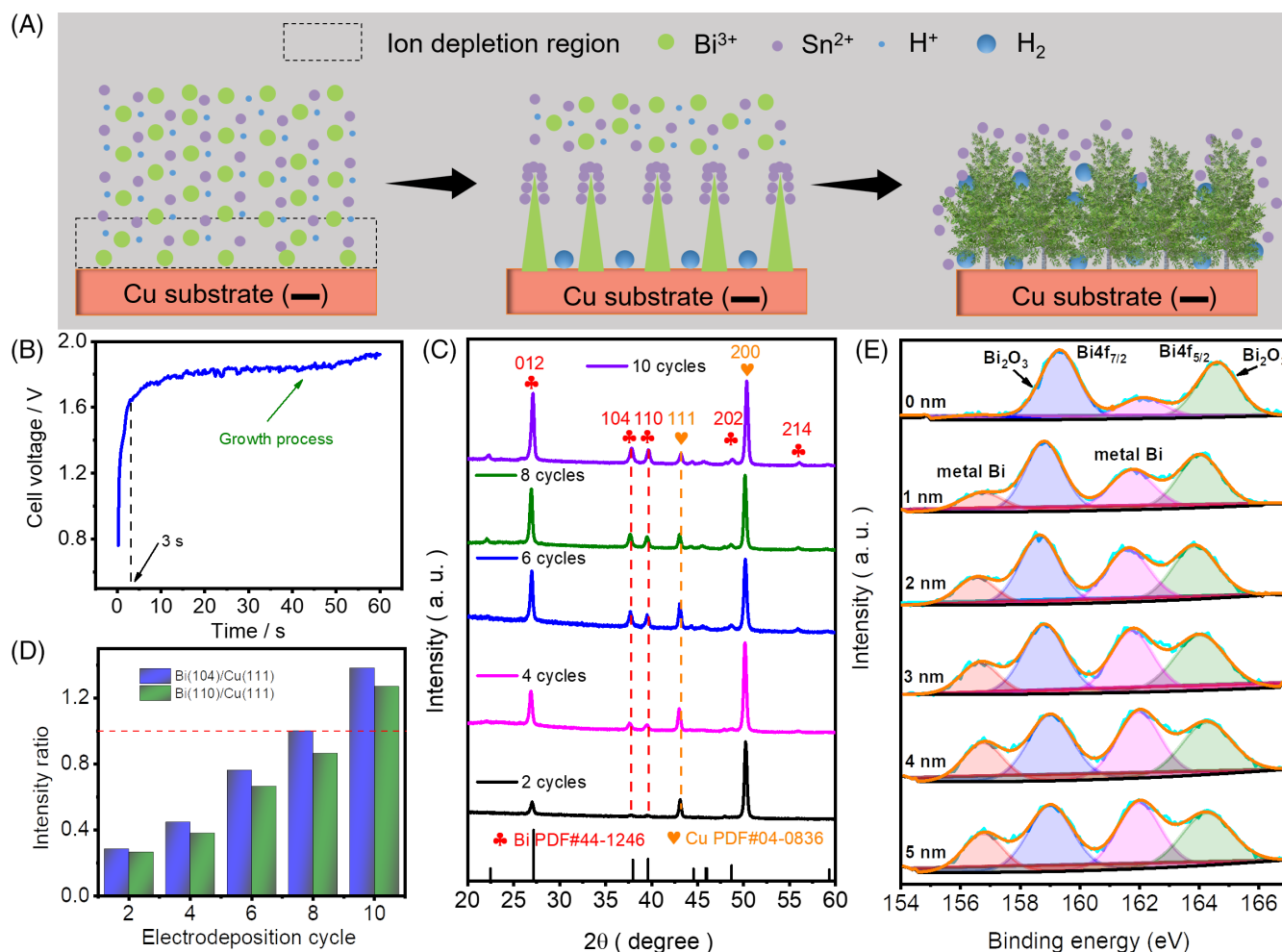


FIGURE 2 (A) The growth mechanism of Sn-doped Bi electrode. (B) The growth curve of Sn-doped Bi electrode during 1 min "on" process. (C) XRD patterns of Sn-doped Bi after different on-off deposition cycles. (D) The intensity ratio of Bi (104)/Cu(111) and Bi(110)/Cu (111) planes in (C). (E) XPS depth-profile of Bi4f

metallic Bi, which nucleate and grow into a dendrite structure, similar to the Ni dendrites obtained from cathodic deposition.³⁷ The strong depletion of metal cations result in a sharp increase in resistance, which corresponds to the rapid voltage rise in the first 3 s (Figure 2B) of the constant current pulse. After that, the growth of Bi dendrites proceeds relatively stable, followed by the deposition of Sn and the generation of H_2 bubble. The agglomeration of hydrogen bubbles prohibits the merge of dendrite even after prolonged deposition, and the bismuth forest will finally be formed (Figures 2A, and S6). However, when the electroplating solution does not contain tin ions, the evolution of dendrite structure becomes different (Figure S7) for pure Bi electrode due to the faster deposition of Bi cations. When the tin cations are replaced by lead (Figure S8) and copper (Figure S9), the dendrite structure disappears due to the formation of isotropic Pb@Bi and Cu@Bi alloys (Figure S10).

Apart from studying the dendrite microstructure, it is also crucial to clarify the growth of bismuth crystal. The X-ray diffraction (XRD) patterns in Figure 2C show three typical peaks at 27.11, 37.86, and 39.64°, which can be ascribed to the (012), (104), and (110) planes of metallic Bi (PDF#44-1246), respectively. Bismuth has a hexagonal structure (PDF#44-1246), which is consistent with the analysis of SAED in Figure 1H. When the on-off deposition cycle is prolonged from 2 to 10, the peak intensities of Bi (104) and (110) planes gradually increase and even exceed the peak intensity of Cu (111) plane from the substrate after 10 cycles (Figures 2D and S11A), which provides strong evidence for the morphology evolution from small branches (Figure S6C,D) to luxuriant bismuth forests (Figure S6I). Except for demonstrating the stable microstructure of Sn-doped Bi after thermal treatment and electrochemical pre-reduction, the stability of crystal structure is also investigated in Figure S11B. The four XRD patterns of Sn-doped Bi after

electrodeposition process, thermal treatment, electrochemical pretreatment and CO₂RR electrolysis show no discernible changes, suggesting the stable crystal structure in nature. Two extra peaks at 43.18 and 50.34° can be assigned to the (111) and (200) planes, respectively, of the metallic Cu (PDF#04-0836) substrate.

The binding energies of Bi4f_{7/2} and Bi4f_{5/2} of Sn-doped Bi (Figure S12) have a positive shift (0.07 eV) to 159.07 and 164.37 eV, respectively, as compared with those of pure Bi crystal, clearly indicating the electron transfer from Bi to Sn. The Bi³⁺ species is dominating on the surface of the two samples because metallic Bi is easily oxidized in air. The XPS depth profile of Sn-doped Bi after thermal treatment in Figure 2E shows that the content of Bi metal species increases with the depth from 0 to 3 nm, and then keeps almost no change from 3 to 5 nm, which demonstrates that the amorphous layer in Figure 1C could be regarded as Bi oxide layer. Besides, the Sn metal species in Figure S13 has almost no change along with the etching depth. The CV curves of pure Bi and Sn-doped Bi electrodes in Figure S14 show that the content of Sn is much lower than that of Bi from an electrochemical perspective.

The catalytic performance of Sn-doped Bi towards CO₂RR is evaluated in Figure 3 and formate is the only liquid product and no other liquid species can be detected by NMR spectrometer (Figure S15). For CO₂RR measurements, the Sn-doped Bi electrode is firstly pretreated to reduce the superficial oxidation species and adsorb K⁺ as mentioned before. The LSV polarization curve of Sn-doped Bi electrode (Figure 3A) in CO₂-saturated condition shows a larger current density than in Ar-saturated condition. It should be noted that the applied potentials of pure Bi and Sn-doped Bi electrodes at 10 mA cm⁻² are -0.80 and -0.73 V versus RHE in CO₂-saturated condition as compared with -0.90 and -0.87 V versus RHE in Ar-saturated one, respectively. Furthermore, the current densities of pure Bi and Sn-doped Bi electrodes at -0.90 V versus RHE are -9.6 and -11.6 mA cm⁻² in Ar-saturated condition compared with -22.2 and -30.2 mA cm⁻² in CO₂-saturated one. This reduced potential (140 mV for Sn-doped Bi and 100 mV for pure Bi) at the same current density and the increased current density (18.6 mA cm⁻² for Sn-doped Bi and 12.6 mA cm⁻² for pure Bi) at the same applied potential in CO₂- and Ar-saturated conditions demonstrate the excellent activity of Sn-doped Bi electrode in CO₂-saturated electrolyte. As shown in Figure 3B, the FE_{HCOO}⁻ of Sn-doped Bi electrode keeps on increasing from 30.3% to 98.2% in a potential window from -0.63 to -0.83 V versus RHE, then maintains more than 95.0% over a broad potential range from -0.83 to -0.93 V versus RHE, and finally decreases in the range of -0.93 to -1.13 V versus RHE. This decreased FE_{HCOO}⁻ in high

potential window is due to the fact that the fast consumption of CO₂ reactant is limited by mass transport, thus favoring the HER. In addition, the FE_{HCOO}⁻ of pure Bi electrode shows the similar trend as Sn-doped Bi electrode with a value of no more than 80.0% at all applied potentials (Figure 3C), suggesting that doping Sn into Bi crystal is an important factor to reach excellent CO₂RR performance. To illustrate which step plays a significant role in formate generation, the Tafel slopes of pure Bi and Sn-doped Bi electrodes are plotted in Figure 3D, wherein the slope value of Sn-doped Bi electrode is 130 mV/dec very close to the 118 mV/dec, demonstrating that the chemical rate-determining step for formate generation is the first electron to form the CO₂*⁻ species. As the smaller value of Tafel slope suggests the lower overpotential in an electrocatalytic reaction, the higher slope value of pure Bi electrode (165 mV/dec) than Sn-doped Bi electrode (Figure 3D) indicates that doping Sn into Bi crystal also accelerates the charge transfer from cathode surface to adsorbed CO₂*⁻ species. To further demonstrate this effect, electrochemical impedance spectroscopy (EIS) is applied to investigate the charge transfer. As shown in Figure 3E, the series resistance (Rs) of Sn-doped Bi electrode is 2.5 Ω, larger than 2.2 Ω of pure Bi electrode, which implies that inserting tin atoms into the lattice of bismuth atoms does slightly decrease the electronic conductivity of bismuth electrode. However, the charge transfer resistance (Rct) of Sn-doped Bi electrode is 1.5 Ω, much lower than 2.1 Ω of pure Bi electrode, which demonstrates again that the charge transfer rate of Sn-doped Bi electrode from cathode surface to CO₂*⁻ species is faster than that of pure Bi electrode. The electrochemical active surface area (ECSA) of Sn-doped Bi electrode is significantly enhanced after thermal treatment and electrochemical pre-reduction (Figure S16), indicating that Bi oxidation and K⁺ adsorption can increase the number of active sites for CO₂RR. Surprisingly, the CO₂RR experiments in catholyte without alkali cation (0.5 M NH₄HCO₃) reveal that the FE_{HCOO}⁻ is no more than 35.0% at full applied potential range from -0.59 to -1.09 V versus RHE (Figure 3F), significantly lower than that in 0.5 M KHCO₃ catholyte (Figure 3B). All the above proves that K⁺ adsorption can greatly alter the electronic structure and adsorption behavior of Sn-doped Bi electrode which promotes a promising selectivity for CO₂RR.

The long-term stability of electrode is very critical for practical applications. There are four main factors so far reported to be responsible for stability attenuation³⁸: catalyst deactivation, the high concentration of produced liquid products in catholyte, the cross-over of produced products from cathode to anode, and the species of anolyte. Therefore, four practical steps are proposed to meliorate the stability issue: designing durable electrode

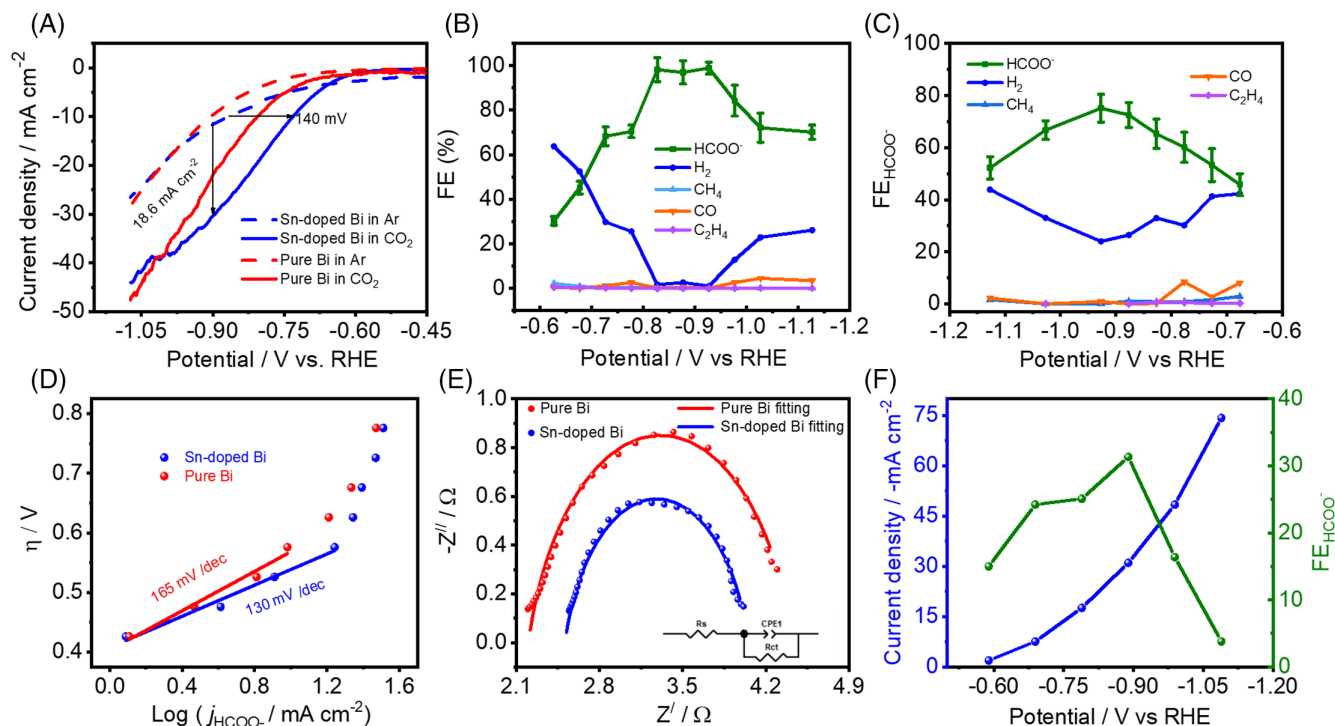


FIGURE 3 (A) LSV of pure Bi and Sn-doped Bi electrodes in Ar and CO₂-saturated 0.5 M KHCO₃ solution at 5 mV s⁻¹ scan rate. (B) and (C) Faradaic efficiencies (FEs) of formate, H₂, CH₄, CO and C₂H₄ by using Sn-doped Bi and pure Bi electrodes, respectively. (D) Tafel plots of Sn-doped Bi and pure Bi electrodes. (E) Electrochemical impedance spectroscopy (EIS) of Sn-doped Bi and pure Bi electrodes. Inset is the equivalent circuit model. (F) FE of formate and current density of Sn-doped Bi electrode in 0.5 M NH₄HCO₃ electrolyte.

configuration,³⁸ refreshing the CO₂ intermediate near the local active sites,³⁹ replacing the separator by bipolar membrane,²¹ and oxidizing small organic molecule in anodic compartment.⁴⁰ Bearing the above four factors in mind, we figured out some strategies to keep the performance of CO₂RR at the superb plateau and revealed the mechanism of stability attenuation by changing the experimental condition. The stability tests in the first part of Figure 4A exhibit a FE_{HCOO⁻} more than 90% during the first 6 h, and the partial current density of formate (~30 mA cm⁻²) obviously oscillates due to the rapid generation of formate with an excellent production rate (487.1 μmol h⁻¹ cm⁻²). Not surprisingly, the FE of formate reduces to less than 80% in the second and third parts (the 24th and 36th hour in the whole experiment) of Figure 4A, which implies that the concentration of produced formate in catholyte has reached a saturated condition, suppressing the further generation of formate. To verify, 0.02 mol/L sodium formate was pre-added in the catholyte before CO₂ electrolysis. As shown in the second part of Figure 4B (red line), the FE of formate after 3 h electrolysis (the 6th hour in the whole experiment) reduces to mere 55.8%, strongly verifying that the high concentration of formate in catholyte is one of the reasons affecting the stability of high FE. This dilemma can be solved by refreshing the catholyte, and hence the FE of

formate can also reach 95.5% in sixth part of Figure 4A (pink line), which also proves that the Sn-doped Bi catalyst does not deactivate after 56 h electrolysis. CV curves of Sn-doped Bi at different stages of electrolysis further confirm the stability of electrode (Figure S17A). Such excellent activity (partial current density), stability (electrolysis time) and selectivity (Faradaic efficiency) of Sn-doped Bi electrode for CO₂RR have surpassed the majority of recently reported Bi-based electrodes as depicted in Figure 4C and Table S1.

It should be mentioned that the FE of formate in cathodic compartment is enhanced as compared with the previous five parts after replacing anolyte by 1 KOH and 1 M glycerol, as shown in the sixth part of Figure 4A (pink line). Intriguingly, the FE of formate in cathode reaches 95.5% and also keeps more than 40% in anode. There are two reasons for the existence of formate in anode: (i) the oxidation of glycerol, and (ii) the cross-over of formate from cathode to anode. The cross-over of formate can be verified from the detection of formate (FE: 8.9%) in the anodic compartment during the first 3 h electrolysis in Figure 4B (black line). To demonstrate the oxidation of glycerol, we changed the anolyte to 1 M KOH and 0.5 M glycerol in the third part of Figure 4B (blue line). As expected, the FE of formate in anode is lowered, as compared with the case in the anolyte of 1 M KOH

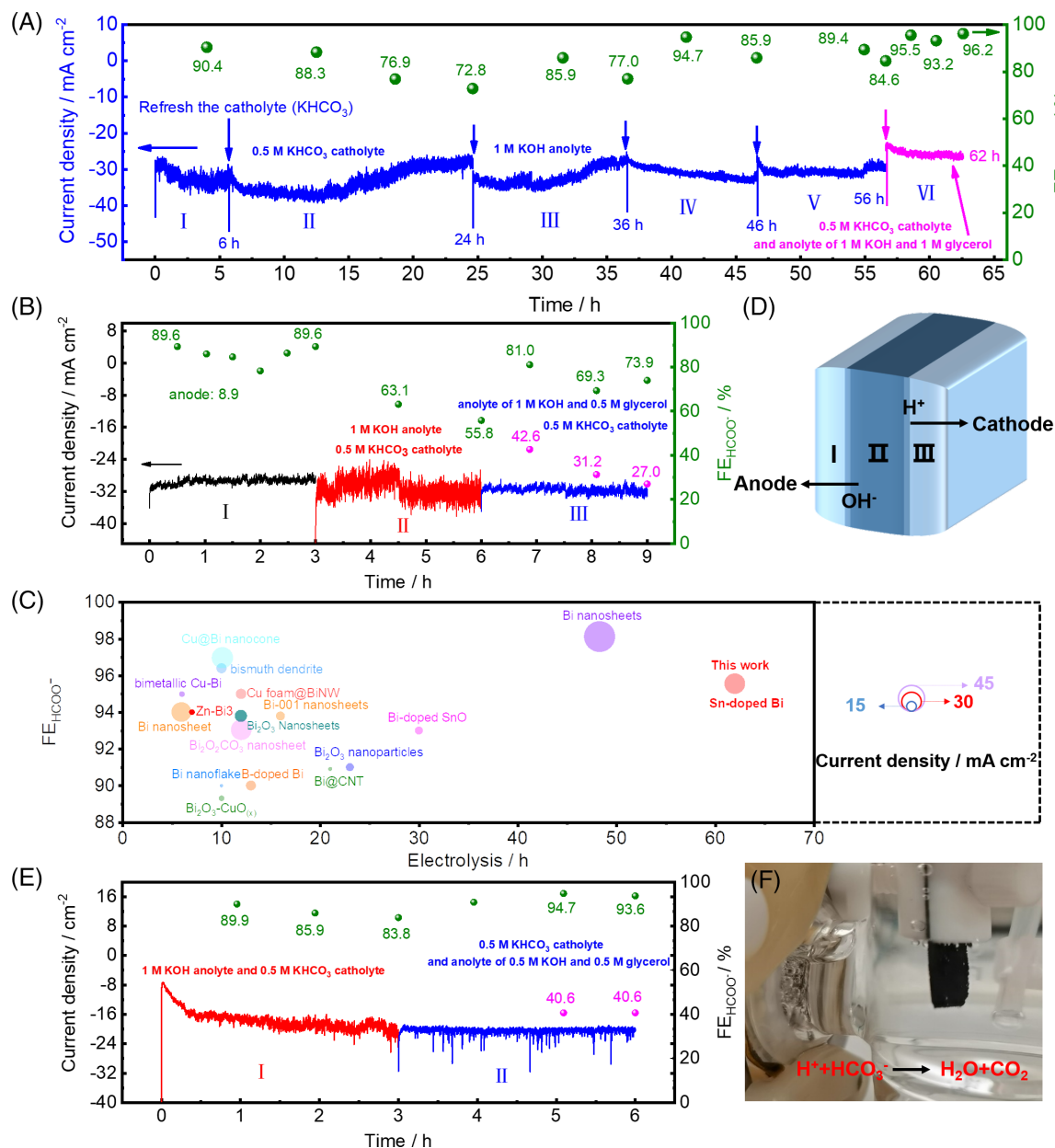


FIGURE 4 (A) Stability test of Sn-doped Bi. The electrolyte was refreshed at the beginning of each part, as indicated by an arrow. (B) Stability test. The first part (black line) was in the same experimental condition as the first five parts of (A). (C) Comparison of FE_{HCOO⁻}, partial current density of formate and electrolysis time of recently reported Bi-based catalysts in CO₂RR. (D) Schematic bipolar membrane, consisted of anion-exchange layer, intermediate buffer layer and cation-exchange layer from left to right. (E) Stability test with the bipolar membrane as the separator. (F) Photographs of cation exchange layer of self-made bipolar membrane in 0.5 M KHCO₃. Bubbles were formed on the surface of cation exchange layer due to the high concentration of H⁺.

and 1 M glycerol (Figure S17B), which confirms the oxidation of glycerol to produce formate in anode. As the theoretical oxidation potential of glycerol is 0.69 V versus SHE, far below 1.23 V versus SHE for OER, the co-production of formate on the anode and cathode compartment is believed to be of great significance to reduce the overall energy utilization efficiency. Video S1 shows that a few gas bubbles are sometimes evolved in cathode compartment, while a great deal of oxygen gas are

emitted in anodic compartment during the first five parts of Figure 4A. However, Video S2 vividly exhibits that no gas bubble is produced in cathodic or anodic compartment during the sixth part of Figure 4A, demonstrating that only liquid products are generated on both sides of the electrode. These megascopic phenomena also support the evidence that the FE of formate in cathode is super high in the sixth part of Figure 4A. As the viscosity of glycerol is higher than water, it is possible that the

glycerol-membrane interface has better ability to prohibit the cross-over of formate from cathode to anode than water-membrane interface. As a consequence, the glycerol-membrane interface inspires us to create a blocking layer for the formate cross-over that is called bipolar membrane as shown in Figure 4D. The detailed preparation of bipolar membrane is described in experimental procedures (Supporting Information). When the self-made bipolar membrane is used as a separator in the first part of Figure 4E (red line), no formate can be detected in anode, which illustrates that the self-made bipolar membrane can effectively prohibit the cross-over of formate. In the second part of Figure 4E (blue line), when the anolyte is refreshed as 0.5 M KOH and 0.5 M glycerol, the FE of formate in cathode maintains more than 93% and the FE of formate in anode keeps around 40%. These results are very promising due to: (i) the marriage of anode and cathode reaction to produce formate on both sides, and (ii) the oxidization of small organic molecule in anode favoring the production of formate in cathode. Nevertheless, there are still challenges to overcome, which are the low FE of formate in anode, the low activity in cathode, and the emergence of CO₂ gas bubbles on the cation exchange layer of bipolar membrane in Figure 4F and Video S3. The emergence of CO₂ gas bubbles is due to the H⁺ ions produced by water dissociation in intermediate buffer layer that penetrate through cation-exchange layer and create an acidic environment at the interface of catholyte and cation-exchange layer. The high concentration of H⁺ at that interface would react with bicarbonate to form CO₂ gas bubbles as shown in Figure 4F.

It should be noted that replacing the catholyte is one of the ways to modify the concentration of formate during long-term stability test but not the best. The best way is to design a flow-cell system for timely refreshing the CO₂ intermediate near the local active sites. According to the above analysis, a flow-cell CO₂RR system is designed as shown in Figure S18A, wherein the core part is our home-made ultrathin liquid reactor with a cathode flow-chamber in a thickness of only 2 mm. The volume of cathode flow-chamber is just 0.8 ml and the flow rate of catholyte is 8 ml/min, which means that the catholyte would be refreshed 10 times within 1 min. Apart from the application of this flow system, the anode catalyst is also a significant factor to determine the overall energy input. Iron on nickel foam (Fe@Ni foam) was synthesized as anode catalyst (Figure S19) to replace platinum foil for oxygen evolution reaction (OER). As displayed in Figure S18B, the applied potential of Fe@Ni foam is only 0.421 V versus SCE (saturated calomel electrode) at 2 mA cm⁻² and that of Pt foil is 0.788 V versus SCE. Eventually, a flow-cell CO₂RR system was assembled with the Sn-doped Bi cathode; the Fe@Ni foam anode; the self-made bipolar membrane separator, and

the home-made ultrathin liquid reactor. Much to our delight, the production rate of formate has a sharp increase from 423.88 μmol h⁻¹ cm⁻² at 50 mA cm⁻² to 1138.12 μmol h⁻¹ cm⁻² at 100 mA cm⁻², and becomes almost saturated at around 1450 μmol h⁻¹ cm⁻² even when the current density is further increased to 150 and 200 mA cm⁻² (Figure S18C). However, more efforts are needed to design a CO₂RR system that meets the industrial standards for future application.

3 | CONCLUSION

In summary, we report a dendritic Sn-doped Bi electrode with stable microstructure and also study the growth mechanism of this peculiar morphology. This dendritic Sn-doped Bi electrode with multiple high-curvature tips would concentrate K⁺ in aqueous electrolyte and in turn enable the CO₂RR in an ultra-high local electric field. Combining the above benefits, the Sn-doped Bi electrode can achieve a considerably high partial current density (30 mA cm⁻²), a high Faradic efficiency of formate (95.55%) and a long-term durability (>60 h). By taking into consideration of the effect of anode reaction, we achieve a synergy of anode and cathode reaction to produce formate on both sides. We eventually assemble a flow-cell CO₂RR system with an ultrathin liquid reactor using the synthesized electrodes and a home-made bipolar membrane to achieve a formate production rate of 1138.1 μmol h⁻¹ cm⁻² at 100 mA cm⁻². The newly designed CO₂RR system with dendritic electrocatalysts, bipolar membrane, and optimized anode reaction shows a great potential for application.

AUTHOR CONTRIBUTIONS

Luwei Peng carried out the experiments and wrote the original draft. Changsheng Chen and Ye Zhu performed the TEM characterization and results analysis. Ruinan He and Nengneng Xu helped do some experiments. Zezhou Lin assisted to polish the pictures. Jinli Qiao and Haitao Huang supervised the whole project, discussed the results, revised the draft, and provided financial support to this work.

ACKNOWLEDGMENTS

This work was supported by the “Scientific and Technical Innovation Action Plan” Basic Research Field of Shanghai Science and Technology Committee (grant numbers 19JC1410500), “the Fundamental Research Funds for the Central Universities and Graduate Student Innovation Fund of Donghua University” (CUSF-DH-D-2021036), the Research Grants Council of the Hong Kong Special Administrative Region, China (PDFS2122-5S02), and the Hong Kong Polytechnic University (YWB6 and YWA1).

CONFLICT OF INTEREST

The authors declare no conflicts of interest.

ORCID

Haitao Huang  <https://orcid.org/0000-0002-3861-2702>

REFERENCES

- Qiao J, Liu Y, Feng H, Zhang J. A review of catalysts for the electroreduction of carbon dioxide to produce low-carbon fuels. *Chem Soc Rev*. 2014;45(17):631.
- Kim S, Dong W, Gim S, et al. Shape-controlled bismuth nano-flakes as highly selective catalysts for electrochemical carbon dioxide reduction to formate. *Nano Energy*. 2017;39(5):44-52.
- Kuang Z, Zhao W, Peng C, et al. Hierarchically porous SnO₂ coupled organic carbon for CO₂ electroreduction. *ChemSusChem*. 2020;13(22):5896-5900.
- Ye K, Cao A, Shao J, et al. Synergy effects on Sn-cu alloy catalyst for efficient CO₂ electroreduction to formate with high mass activity. *Sci Bull*. 2020;65(9):711-719.
- Peng L, Wang Y, Masood I, et al. Self-growing Cu/Sn bimetallic electrocatalysts on nitrogen-doped porous carbon cloth with 3D-hierarchical honeycomb structure for highly active carbon dioxide reduction. *Appl Catal B*. 2020;264:118447.
- Ma W, Xie S, Zhang X, et al. Promoting electrocatalytic CO₂ reduction to formate via sulfur-boosting water activation on indium surfaces. *Nat Commun*. 2019;10(1):892.
- Pander J, Lum J, Yeo B. The importance of morphology on the activity of lead cathodes for the reduction of carbon dioxide to formate. *J Mater Chem A*. 2019;7(8):4093-4101.
- Ye K, Zhou Z, Shao J, Lin L, Bao X. In situ reconstruction of hierarchical Sn-cu/SnOx Core/Shell catalyst for high-performance CO₂ electroreduction. *Angew Chem Int Ed*. 2020;59(12):4814-4821.
- Li L, Cai F, Qi F, Ma D. Cu nanowire bridged bi nanosheet arrays for efficient electrochemical CO₂ reduction toward formate. *J Alloys Compd*. 2020;841:155789.
- Liu Y, Wang H, Zhao T, et al. Schottky barrier induced coupled Interface of electron-rich N-doped carbon and electron-deficient Cu: in-built Lewis acid-Base pairs for highly efficient CO₂ fixation. *J Am Chem Soc*. 2019;141(1):38-41.
- Xing Y, Kong X, Guo X, et al. Bi@Sn core-shell structure with compressive strain boosts the electroreduction of CO₂ into formic acid. *Adv Sci*. 2020;7(22):1902989.
- Ma T, Wu Z, Wu H, et al. Engineering bi-Sn interface in bimetallic aerogel with 3D porous structure for highly selective electrocatalytic CO₂ reduction to HCOOH. *Angew Chem Int Ed*. 2021;133(22):12662-12667.
- Huang J, Guo X, Huang X, Wang L. Metal (Sn, bi, Pb, cd) in-situ anchored on mesoporous hollow kapok-tubes for outstanding electrocatalytic CO₂ reduction to formate. *Electrochim Acta*. 2019;325:134923.
- Gong Q, Ding P, Xu M, et al. Structural defects on converted bismuth oxide nanotubes enable highly active electrocatalysis of carbon dioxide reduction. *Nat Commun*. 2019;10(1):2807.
- Wen G, Lee D, Ren B, et al. Orbital interactions in bi-Sn bimetallic electrocatalysts for highly selective electrochemical CO₂ reduction toward formate production. *Adv Energy Mater*. 2018;8:1870138.
- Zhao X, Chen Q, Zhuo D, Lu J, Guo G. Oxygen vacancies enriched bi based catalysts for enhancing electrocatalytic CO₂ reduction to formate. *Electrochim Acta*. 2021;367:137478.
- Yang X, Deng P, Liu D, et al. Partial sulfuration-induced defect and interface tailoring on bismuth oxide for promoting electrocatalytic CO₂ reduction. *J Mater Chem A*. 2020;8(5):2472-2480.
- Koh J, Won D, Eom T, et al. Facile CO₂ electro-reduction to formate via oxygen bidentate intermediate stabilized by high-index planes of bi dendrite catalyst. *ACS Catal*. 2017;7(8):5071-5077.
- Liu M, Pang Y, Zhang B, et al. Enhanced electrocatalytic CO₂ reduction via field-induced reagent concentration. *Nature*. 2016;537(7620):382-386.
- An P, Wei L, Li H, et al. Enhancing CO₂ reduction by suppressing hydrogen evolution with polytetrafluoroethylene protected copper nanoneedles. *J Mater Chem A*. 2020;8(31):15936-15941.
- Yan Z, Hitt J, Zeng Z, Hickner M, Mallouk T. Improving the efficiency of CO₂ electrolysis by using a bipolar membrane with a weak-acid cation exchange layer. *Nat Chem*. 2021;13(1):33-40.
- Amorim I, Xu J, Zhang N, et al. Dual-phase CoP-CoTe₂ nanowires as an efficient bifunctional electrocatalyst for bipolar membrane-assisted acid-alkaline water splitting. *Chem Eng J*. 2021;420:130454.
- Ogunbemi E, Wilberforce T, Ijaodola O, Thompson J, Olabi A. Review of operating condition, design parameters and material properties for proton exchange membrane fuel cells. *Int J Energy Res*. 2021;45(2):1227-1245.
- Salvatore D, Weekes D, He J, et al. Electrolysis of gaseous CO₂ to CO in a flow cell with a bipolar membrane. *ACS Energy Lett*. 2018;3(1):149-154.
- Kibria M, Edwards J, Gabardo C, et al. Electrochemical CO₂ reduction into chemical feedstocks: from mechanistic electrocatalysis models to system design. *Adv Mater*. 2019;31(31):1807166.
- Bushuyev O, Luna P, Dinh C, et al. What should we make with CO₂ and how can we make it? *Joule*. 2018;2(5):825-832.
- Han N, Wang Y, Yang H, et al. Ultrathin bismuth nanosheets from in situ topotactic transformation for selective electrocatalytic CO₂ reduction to formate. *Nat Commun*. 2018;9(1):1320.
- Li F, Thevenon A, Rosas-Hernandez A, et al. Molecular tuning of CO₂-to-ethylene conversion. *Nature*. 2020;577(7791):509-513.
- Weng L, Bell A, Weber A. Towards membrane-electrode assembly systems for CO₂ reduction: a modeling study. *Energ Environ Sci*. 2019;12(6):1950-1968.
- Ma M, Clark EL, Therkildsen K, Dalsgaard S, Chorkendorff I, Seger B. Insights into the carbon balance for CO₂ electroreduction on Cu using gas diffusion electrode reactor designs. *Energ Environ Sci*. 2020;13(3):977-985.
- Díaz-Sainz G, Alvarez-Guerra M, Ávila-Bolívar B, Solla-Gullón J, Montiel V, Irabien A. Improving trade-offs in the figures of merit of gas-phase single-pass continuous CO₂ electrocatalytic reduction to formate. *Chem Eng J*. 2021;405:126965.
- Ramdin M, Morrison A, de Groen M, et al. High pressure electrochemical reduction of CO₂ to formic acid/formate: a comparison between bipolar membranes and cation exchange membranes. *Ind Eng Chem Res*. 2019;58(5):1834-1847.
- Xia C, Zhu P, Jiang Q, et al. Continuous production of pure liquid fuel solutions via electrocatalytic CO₂ reduction using solid-electrolyte devices. *Nat Energy*. 2019;4(9):776-785.

34. Fan L, Xia C, Zhu P, Lu Y, Wang H. Electrochemical CO₂ reduction to high-concentration pure formic acid solutions in an all-solid-state reactor. *Nat Commun*. 2020;11(1):3633.
35. Ma D, Jin T, Xie K, Huang H. An overview of flow cell architecture design and optimization for electrochemical CO₂ reduction. *J Mater Chem A*. 2021;9(37):20897-20918.
36. Liang S, Altaf N, Huang L, Gao Y, Wang Q. Electrolytic cell design for electrochemical CO₂ reduction. *J CO₂ Util*. 2020;35(9):90-105.
37. Liu Y, Fu N, Zhang G, Lu W, Zhou L, Huang H. Ni@NiO core/shell dendrites for ultra-long cycle life electrochemical energy storage. *J Mater Chem A*. 2016;4(39):15049-15056.
38. Popović S, Smiljanić M, Jovanović P, Vavra J, Buonsanti R, Hodnik N. Stability and degradation mechanisms of copper-based catalysts for electrochemical CO₂ reduction. *Angew Chem Int Ed*. 2020;132(35):14844-14854.
39. Peng L, Wang Y, Wang Y, et al. Separated growth of bi-cu bimetallic electrocatalysts on defective copper foam for highly converting CO₂ to formate with alkaline anion-exchange membrane beyond KHCO₃ electrolyte. *Appl Catal B*. 2021;288:120003.
40. Nazir R, Kumar A, Ali Saleh Saad M, Ali S. Development of CuAg/Cu₂O nanoparticles on carbon nitride surface for methanol oxidation and selective conversion of carbon dioxide into formate. *J Colloid Interf Sci*. 2020;578(75):726-737.

SUPPORTING INFORMATION

Additional supporting information can be found online in the Supporting Information section at the end of this article.

How to cite this article: Peng L, Chen C, He R, et al. Tin-doped bismuth dendrites for highly efficient electrocatalytic reduction of CO₂ by using bipolar membrane in ultrathin liquid reactor. *EcoMat*. 2022;4(6):e12260. doi:[10.1002/eom2.12260](https://doi.org/10.1002/eom2.12260)